Proceedings of ALGORITMY 2020
pp. 81–90

FLUID-STRUCTURE-ACOUSTIC INTERACTION PROBLEM IN MODELLING OF HUMAN VOCAL FOLDS VIBRATION*

JAN VALÁŠEK†, PETR SVÁČEK† , AND JAROMÍR HORÁČEK‡

Abstract. This paper studies vibroacoustic sound produced by self-oscillating human vocal folds model as one of major sound source responsible for human phonation. The human phonation is a complex phenomenon described by interaction of three physical fields – elastic body deformation, fluid flow and acoustics, and their mutual couplings. Therefore it is sometimes referred as fluid-structure-acoustic interaction (FSAI) problem. Here we present FSI problem modelled by linear elasticity theory (vocal fold) and the viscous incompressible airflow modelled by Navier-Stokes equations due to typical low flow velocities of small Mach number. The arbitrary Lagrangian-Euler method (ALE) for the purpose of numerical simulation of the time varying computational domain is applied. In order to model one sound source mechanism of the human phonation the vibroacoustic problem is solved in larger acoustic domain including vocal tract model. The sound source considered in this model is the normal acceleration of the vibrating vocal folds boundary. The numerical models are based on the finite element method. The results of vibroacoustic problem are shown and analyzed.

Key words. flow-induced vibration; 2D incompressible Navier-Stokes equations; linear elasticity; vibroacoustics;

AMS subject classifications. (MSC 2010: 65N30, 65M60, 74B05, 74F10, 76D05, 76G99.)

1. Introduction. The human phonation is a complex phenomenon described by interaction of three physical fields – elastic body deformation, fluid flow and acoustics, and their mutual couplings. Therefore it is sometimes referred as fluid-structure-acoustic interaction (FSAI) problem, see e.g. [6]. The sound sources are produced by three main mechanisms – the modulated air stream emerged by repetitively opening and closing glottis, the eddy-induced sound of turbulent flow structures and the sound from the vibrating vocal folds (VFs), see [1]. Although the sound of vibroacoustic origin is hypothesized to be small, see [14, 1], nevertheless recent laboratory measurements of VF replica combined with numerical modelling [7] showed that the acoustic emission could be significant. It motivates our study of vibroacoustic problem.

The presented FSAI mathematical model of phonation is composed of linear elasticity theory (vocal fold vibration), fluid flow described by viscous incompressible Navier-Stokes equations and the classical acoustic wave equation with prescribed normal acceleration at the vocal fold boundary. The arbitrary Lagrangian-Euler method (ALE) is applied for the purpose of including the time varying computational domain into fluid flow model. In order to simulate vibration-borne sound of the human phonation the vibroacoustic problem is solved in larger acoustic domain including vocal tract model, which acts as a filter of sound waves generated in the larynx, see [11].

We disregard in this study the influence of acoustic pressure on the vocal fold vibration what allows to decouple the acoustic problem and the fluid-structure interaction (FSI) problem. For the modelling of open boundary problem at the vocal

*This work was supported by Grant No.: GA 19-04477S of the Czech Science Foundation and by the Grant No. SGS19/154/OHK2/3T/12 of the Grant Agency of the CTU in Prague.

†Department of Technical Mathematics, FME, CTU in Prague, Karlovo náměstí 13, 121 35, Praha 2, CZ (Jan.Valasek1@fs.cvut.cz).

‡Institute of Thermomechanics, Czech Academy of Sciences, Dolejškova 5, 182 00, Praha 8, CZ.

tract model outlet the perfectly matched layer (PML) technique is applied, see e.g. [5]. The numerical approximation of all three subproblems is based on the finite element method (FEM), particularly in the fluid flow case the advanced stabilization technique is used. The FSI numerical solution, implemented as strongly coupled partitioned scheme, is presented and analyzed. The results of vibroacoustic problem are shown including the sound pressure level (SPL) at the vocal tract end.

The paper is structured as follows: In the next section the mathematical model of the three physical problems as well as their interactions are given. Then the numerical methods are described. In the end the numerical results of FSI and FSAI problems are presented.

2. Mathematical model. We consider a two-dimensional FSAI problem. First, the domain of FSI problem is introduced and the acoustic domain is described later. The FSI domain is composed of the reference elastic structure domain $\Omega^s_{\rm ref}$ and the reference fluid domain $\Omega^f_{\rm ref}$, see Figure 2.1. The motion of the elastic body is described in Lagrangian coordinates, i.e. the computational domain Ω^s does not depend on time and it is identical with its reference domain $\Omega^s := \Omega^s_{\rm ref}$.

The reference fluid domain $\Omega^f_{\rm ref}$ is chosen as the domain filled with fluid at the time instant $t = 0$ with the common interface $\Gamma_{\rm W_{ref}} = \Gamma_{\rm W_0}$ between the fluid and the structure domain. The reference domain $\Omega^f_{\rm ref}$ is mapped at any time instant t to the deformed domain Ω^f_t with the interface $\Gamma_{\rm W_t}$ using an ALE mapping A_t.

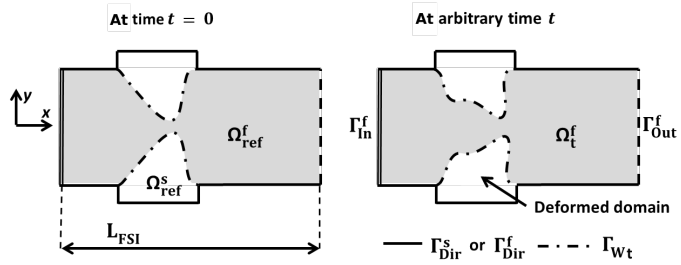

FIG. 2.1. *Scheme of the FSI domain composed of elastic structure domain Ω^s and fluid domain Ω^f. The FSI domain in reference state is shown on the left and the domain undergoing a deformation at arbitrary time t is displayed on the right. The following boundaries are marked: the inlet $\Gamma^f_{\rm In}$, the outlet $\Gamma^f_{\rm Out}$, the walls $\Gamma^f_{\rm Dir}$, $\Gamma^s_{\rm Dir}$ and the interface $\Gamma_{\rm W_t}$.*

2.1. Elastic structure. The structure deformation described by displacement $\mathbf{u}(X,t) = (u_1, u_2)$ of any point $X \in \Omega^s$ obeys following partial differential equations

$$\rho^s \frac{\partial^2 u_i}{\partial t^2} - \frac{\partial \tau^s_{ij}}{\partial X_j} = 0, \qquad \text{in } \Omega^s \times (0,\mathrm{T}), \quad (i = 1,2), \tag{2.1}$$

where ρ^s is the structure density and τ_{ij} are the components of the Cauchy stress tensor. The stress tensor components can be expressed with the help of the Hooke's law and assuming the isotropic body as

$$\tau^s_{ij} = \lambda^s \mathrm{div}\ \mathbf{u}\, \delta_{ij} + 2\mu^s e^s_{ij}(\mathbf{u}), \tag{2.2}$$

where δ_{ij} denotes Kronecker's delta and $e^s_{ij}(\mathbf{u}) = \frac{1}{2}\left(\frac{\partial u_j}{\partial X_i} + \frac{\partial u_i}{\partial X_j}\right)$ is the small strain tensor. The parameters λ^s, μ^s are the Lamé coefficients, see e.g. [8]. Problem (2.1) is

supplied with the zero initial and the following boundary conditions

$$\begin{aligned} &\text{a)} && \mathbf{u}(X,t) = \mathbf{u}_{\mathrm{Dir}}(X,t) \quad \text{for } X \in \Gamma^s_{\mathrm{Dir}}, \\ &\text{b)} && \tau^s_{ij}(X,t)\, n^s_j(X) = q^s_i(X,t), \qquad \text{for } X \in \Gamma^s_{\mathrm{W_{ref}}}, \end{aligned} \tag{2.3}$$

where the $\Gamma_{\mathrm{W_{ref}}}, \Gamma^s_{\mathrm{Dir}}$ are disjoint parts of the boundary $\partial\Omega^s$ and $n^s_j(X)$ are the components of the outward unit normal to $\partial\Omega^s$, see Figure 2.1.

2.2. ALE method. The ALE method is based on the use of ALE mapping A_t which maps the reference fluid domain Ω^f_{ref} onto the deformed domain Ω^f_t at any time instant t, i.e. $\Omega^f_t = A_t(\Omega^f_{ref})$. We assume, that ALE mapping is sufficiently smooth, diffeomorphic mapping and it satisfies at any $t \in [0, \mathrm{T}]$

$$A_t(\partial\Omega^f_{\mathrm{ref}} \backslash \Gamma_{\mathrm{W_{ref}}}) = \partial\Omega^f_{\mathrm{ref}} \backslash \Gamma_{\mathrm{W_{ref}}}, \quad A_t(\Gamma_{\mathrm{W_{ref}}}) = \Gamma_{\mathrm{W_t}}, \tag{2.4}$$

where the location of $\Gamma_{\mathrm{W_t}}$ is given by the displacement of the interface $\Gamma_{\mathrm{W_{ref}}}$ at time instant t. The ALE domain velocity $\mathbf{w}_D$ representing the velocity of a point x with a given reference $X \in \Omega^f_{\mathrm{ref}}$ is defined by

$$\mathbf{w}_D(x,t) = \hat{\mathbf{w}}_D(A_t^{-1}(x), t), \quad \text{where } x = A_t(X) \in \Omega^f_t, \tag{2.5}$$

and $\hat{\mathbf{w}}_D(X,t) = \frac{\partial}{\partial t} A_t(X)$, for $t \in (0, \mathrm{T})$ and $X \in \Omega^f_{\mathrm{ref}}$. Finally, the ALE derivative, i.e. the time derivative with respect to a fixed reference $X \in \Omega^f_{\mathrm{ref}}$, satisfies (see e.g. [3])

$$\frac{D^A}{Dt} f(x,t) = \frac{\partial f}{\partial t}(x,t) + \mathbf{w}_D(x,t) \cdot \nabla f(x,t). \tag{2.6}$$

2.3. Fluid flow. The viscous incompressible fluid flow is modelled in the time dependent domain Ω^f_t by Navier-Stokes equations in the ALE form (see details [3])

$$\frac{D^A \mathbf{v}}{Dt} + ((\mathbf{v} - \mathbf{w}_D) \cdot \nabla)\mathbf{v} - \nu^f \Delta \mathbf{v} + \nabla p = \mathbf{0}, \quad \mathrm{div}\ \mathbf{v} = 0 \quad \text{in } \Omega^f_t, \tag{2.7}$$

where $\mathbf{v}(x,t)$ is the fluid velocity, p denotes the kinematic pressure and ν^f is the kinematic fluid viscosity.

The equations (2.7) are equipped with the zero initial condition and with the following boundary conditions

$$\begin{aligned} &\text{a)} && \mathbf{v}(x,t) = \mathbf{w}_D(x,t) && \text{for } x \in \Gamma^f_{\mathrm{Dir}} \cup \Gamma_{\mathrm{W_t}}, \\ &\text{b)} && (p - p_{\mathrm{ref}})\mathbf{n}^f - \nu^f \frac{\partial \mathbf{v}}{\partial \vec{n}^f} = -\frac{1}{2}\mathbf{v}(\mathbf{v} \cdot \mathbf{n}^f)^- && \text{on } \Gamma^f_{\mathrm{In}} \cup \Gamma^f_{\mathrm{Out}}, \end{aligned} \tag{2.8}$$

where the vector $\mathbf{n}^f = (n^f_j)$ denotes the outward unit normal to the boundary $\partial\Omega^f$, p_{ref} denotes a reference pressure and by $(\alpha)^-$ the negative part of real number $\alpha \in \mathbb{R}$ is denoted, i.e. $(\alpha)^- = \min\{0, \alpha\}$. The condition (2.8 b) is the modified do-nothing boundary condition according to [2], which increases the stability in the case of a backward inlet through the outlet boundary. For the outlet part of boundary the reference pressure is chosen $p_{\mathrm{ref}} = 0$, while for the inlet we denote $p_{\mathrm{in}} := p_{\mathrm{ref}} > 0$.

2.4. Acoustics. The acoustic problem is modelled in the acoustic domain Ω^a, see Figure 2.2. The domain Ω^a consists of two parts $\overline{\Omega^a} = \overline{\Omega^a_{\rm prop}} \cup \overline{\Omega^a_{\rm pml}}$, where the domain of acoustic propagation $\Omega^a_{\rm prop}$ is comprised of two subsets $\Omega^a_{\rm src}$ and $\Omega^a_{\rm air}$, i.e. $\overline{\Omega^a_{\rm prop}} = \overline{\Omega^a_{\rm src}} \cup \overline{\Omega^a_{\rm air}}$. The domain $\Omega^a_{\rm src}$ is equal to the reference fluid domain, i.e. $\Omega^a_{\rm src} = \Omega^f_{\rm ref}$, and the acoustic sources are located at vibrating structure interface $\Gamma_{\rm W_{ref}} \subset \Omega^f_{\rm ref}$. The domain $\Omega^a_{\rm air}$ constitutes a model of the vocal tract behind the glottis up to mouth including a free field region, i.e. the outer space. Finally the PML domain $\Omega^a_{\rm pml}$ closes the free field part of domain $\Omega^a_{\rm air}$ and the outgoing sound waves are here damped. We assume, that the boundary $\partial\Omega^a$ is piecewise Lipschitz continuous.

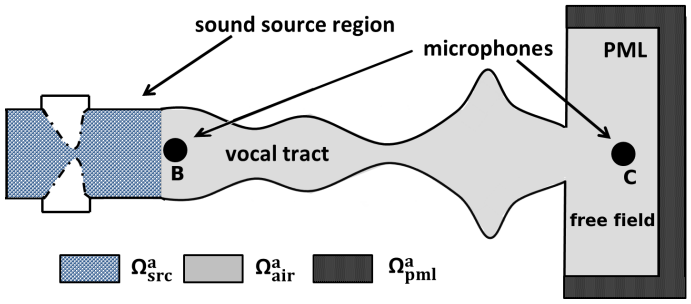

FIG. 2.2. *Scheme of acoustic domain composed of three parts – the sound source region, the vocal tract together with the free field, which is enclosed by the PML region. The positions of microphones B and C are shown.*

The sound propagation through homogeneous medium at rest is described by the wave equation for acoustic pressure $p^a(X,t)$, see e.g. [6],

$$\frac{1}{c_0^2}\frac{\partial^2 p^a}{\partial t^2} - \Delta p^a = f^a(X,t), \qquad \text{in } \Omega^a_{\rm prop} \times (0,{\rm T}), \tag{2.9}$$

where c_0 is the speed of sound and function f^a describes sound sources (due to airflow). In this paper these sources are omitted , i.e. $f^a = 0$, and only sound sources due to vibrating interface $\Gamma_{\rm W_{ref}}$ of the elastic body are considered. Equation (2.9) is equipped with zero initial conditions and following boundary conditions

$$\text{a)} \qquad \frac{\partial p^a}{\partial \mathbf{n}^a}(X,t) = 0, \qquad \text{for } X \in \partial\Omega^a \setminus \Gamma_{\rm W_{ref}}, \tag{2.10}$$

$$\text{b)} \qquad \frac{\partial p^a}{\partial \mathbf{n}^a}(X,t) = -\rho_0^f \frac{\partial u_n}{\partial t}, \qquad \text{for } X \in \Gamma_{\rm W_{ref}},$$

where ρ_0^f is the fluid density, u_n denotes wall normal velocity and vector $\mathbf{n}^a = (n_j^a)$ is unit outer normal to $\partial\Omega^a$. The condition (2.10 a) is so called sound hard boundary condition and it represents fully reflecting walls. The second condition (2.10 b) generalizes the sound hard condition for the vibrating boundary, which creates acoustic emissions from the vocal fold surface, see e.g. [6].

The "open boundary" is modelled using PML technique realized by few additional layers of elements (domain $\Omega^a_{\rm pml}$) where the sound waves are effectively damped to zero by solution of modified wave equation, see e.g. [6]. A suitable choice of parameters is used in order to avoid the reflection at the interface between $\Omega^a_{\rm pml}$ and $\Omega^a_{\rm air}$, see [5].

2.5. Coupling conditions. First the coupling conditions for FSI problem are stated. The fluid and structure problems are coupled together with the aid of the interface boundary conditions prescribed at the interface $\Gamma_{\mathrm{W_t}}$ whose position is determined in terms of the displacement $\mathbf{u}$ at time t as

$$\Gamma_{\mathrm{W_t}} = \left\{ x \in \mathbb{R}^2 |\, x = X + \mathbf{u}(X,t),\, X \in \Gamma_{\mathrm{W_{ref}}} \right\}. \tag{2.11}$$

At the interface $\Gamma_{\mathrm{W_t}}$ the kinematic condition is prescribed as given by equation (2.8 a). The (dynamic) boundary condition at the interface $\Gamma_{\mathrm{W_{ref}}}$ has the form of equation (2.3 b), where the vector of acting aerodynamic forces $\mathbf{q}^s$ with components q_i^s is given by

$$q_i^s = \sum_{j=1}^{2} \rho^f \left(p\delta_{ij} - \nu^f \left(\frac{\partial v_i}{\partial x_j} + \frac{\partial v_j}{\partial x_i} \right) \right) n_j^f(x). \tag{2.12}$$

Further, the structure-acoustic coupling is realized by prescription of velocity continuity in normal direction at the interface $\Gamma_{\mathrm{W_{ref}}}$, which leads to the boundary condition for acoustic pressure p^a as given by equation (2.10 b), i.e.

$$\frac{\partial p^a}{\partial \mathbf{n}^a}(X,t) = -\rho^f \frac{\partial^2 \mathbf{u}(X,t)}{\partial t^2} \cdot \mathbf{n}^a, \qquad x \in \Gamma_{\mathrm{W_{ref}}},\ t \in (0,\mathrm{T}). \tag{2.13}$$

Similarly, the boundary condition which follows from the requirement of stress continuity in normal direction at the interface $\Gamma_{\mathrm{W_{ref}}}$

$$\tau_{ij}^s\, n_j^s = q_i^s + q_i^a, \tag{2.14}$$

where $q_i^a(X,t) = p^{\mathrm{va}} n_i^s$. However the acoustic pressure is usually much smaller compared to the aerodynamic forces (high sound intensity of 100 dB corresponds to value of $p^a = 2\,\mathrm{Pa}$) thus the coupling represented by q_i^a is neglected here, see e.g. [6].

3. Numerical modelling. The FEM is used for spatial discretization of all three considered subproblems (2.1), (2.7) and (2.9). For the purpose of time discretization the time interval $[0,\mathrm{T}]$ is divided into N equidistant parts Δt, i.e. $t_n = n\Delta t, \Delta t = \frac{T}{N}$ for $n = \{0,1,\ldots,N\}$.

3.1. Elastic structure. The FE discretization is based on the weak reformulation of equation (2.1), i.e. Eq. (2.1) is multiplied by a test function $\boldsymbol{\psi}$ from the space $\mathbf{V} = \{\mathbf{f} \in \mathbf{H}^1(\Omega^s) | \mathbf{f} = \mathbf{0} \text{ on } \Gamma^s_{\mathrm{Dir}}\}$, integrated over the whole domain Ω^s and the Green's theorem is used with the boundary condition (2.3 b) applied. The weak formulation is then given by

$$\left(\rho^s \frac{\partial^2 \mathbf{u}}{\partial t^2}, \boldsymbol{\psi} \right)_{\Omega^s} + \left(\lambda^s (\mathrm{div}\ \mathbf{u})\, \mathbb{I} + 2\mu^s \mathbf{e}^s(\mathbf{u}), \mathbf{e}^s(\boldsymbol{\psi}) \right)_{\Omega^s} = \left(\mathbf{q}^s, \boldsymbol{\psi} \right)_{\Gamma_{\mathrm{W_{ref}}}}, \tag{3.1}$$

where the brackets $(\cdot,\cdot)_{\mathcal{D}}$ denotes the dot product in the Lebesque spaces $L^2(\mathcal{D})$ or $\mathbf{L}^2(\mathcal{D})$. We say that $\mathbf{u} \in \mathbf{H}^1(\Omega^s)$ is a weak solution of equation (2.1) if it fulfills the boundary condition (2.3 a) and equation (3.1) is satisfied for any test function $\boldsymbol{\psi} \in \mathbf{V}$.

The space $\mathbf{V}$ is approximated by it's finite element subspace $\mathbf{V}_h \subset \mathbf{V}$ with $\dim V_h = N_h$. The approximate solution $\mathbf{u}_h \in \mathbf{V}_h$ is expressed using basis functions $\boldsymbol{\psi}_j$ of space $\mathbf{V}_h$ in the form $\mathbf{u}_h(X,t) = \sum_{j=1}^{N_h} \alpha_j(t) \boldsymbol{\psi}_j(X)$. Equation (3.1) is rewritten using this form as

$$\mathbb{M}\ddot{\boldsymbol{\alpha}} + \mathbb{C}\dot{\boldsymbol{\alpha}} + \mathbb{K}\boldsymbol{\alpha} = \mathbf{b}(t), \tag{3.2}$$

where the vector $\mathbf{b}(t)$ has components $b_i(t) = (\mathbf{q}^s, \boldsymbol{\psi}_i)_{\Gamma_{\mathrm{W_{ref}}}}$ and the elements of matrices $\mathbb{M} = (m_{ij}), \mathbb{K} = (k_{ij})$ are given by

$$m_{ij} = (\rho^s \boldsymbol{\psi}_j, \boldsymbol{\psi}_i)_{\Omega^s}, \quad k_{ij} = (\lambda^s (\mathrm{div}\ \boldsymbol{\psi}_j)\, \delta_{ij} + 2\mu^s \mathbf{e}^s(\boldsymbol{\psi}_j), \mathbf{e}^s(\boldsymbol{\psi}_i))_{\Omega^s}. \tag{3.3}$$

The model of proportional damping is utilized, i.e. the additionally added matrix $\mathbb{C}$ is chosen as $\mathbb{C} = c_1\mathbb{M} + c_2\mathbb{K}$ with suitably chosen parameters c_1, c_2. The resulting system of second order ordinary differential equations (3.2) is time discretized by Newmark method, see [3].

3.2. Fluid flow. The fluid flow problem equation (2.7) is first discretized in time. The ALE derivative at t_{n+1} is replaced by the backward difference formula of second order (BDF2)

$$\frac{D^A \mathbf{v}}{Dt}(t_{n+1}) \approx \frac{3\mathbf{v}^{n+1} - 4\overline{\mathbf{v}}^n + \overline{\mathbf{v}}^{n-1}}{2\Delta t}, \tag{3.4}$$

where $\mathbf{v}^i \approx \mathbf{v}(\cdot, t_i)$ and for fixed time instant t_{n+1} we denote $\overline{\mathbf{v}}^i(x) = \mathbf{v}^i(A_{t_i}(A^{-1}_{t_{n+1}}(x))$ for $i \in \{n-1, n\}$ and $x \in \Omega^f_{t_{n+1}}$. In what follows we are concerned with the discretization at time $t = t_{n+1}$, and thus the time index $^{n+1}$ is omitted, i.e. we write $\Omega^f := \Omega^f_{t_{n+1}}$.

For weak formulation of (2.7) the function spaces for velocity and pressure are chosen as $\mathbf{X} = \{\mathbf{f} \in \mathbf{H}^1(\Omega^f) |\, \mathbf{f} = \mathbf{0}$ on $\Gamma^f_{\mathrm{Dir}} \cup \Gamma^f_{\mathrm{W_{t_{n+1}}}}\}$ and $M = L^2(\Omega^f)$, respectively. The weak form of (2.7) reads: find $V = (\mathbf{v}, p) \in \mathbf{H}^1(\Omega^f) \times M$, which approximately satisfies boundary condition (2.8 a) and

$$a(V, \Phi) + c(V; V, \Phi) = f(\Phi) \tag{3.5}$$

holds for any $\Phi = (\boldsymbol{\varphi}, q) \in \mathbf{X} \times M$. The forms $a(\cdot,\cdot), c(\cdot;\cdot,\cdot)$ and the functional $f(\cdot)$ are given by

$$\begin{aligned}
a(V, \Phi) &= \left(\frac{3\mathbf{v}}{2\Delta t}, \boldsymbol{\varphi}\right)_{\Omega^f} + \nu^f (\nabla \mathbf{v}, \nabla \boldsymbol{\varphi})_{\Omega^f} - (p, \mathrm{div}\, \boldsymbol{\varphi})_{\Omega^f} + (q, \mathrm{div}\, \mathbf{v})_{\Omega^f}, \\
c(V^*; V, \Phi) &= \frac{1}{2}(((\mathbf{v}^* - 2\mathbf{w}_D) \cdot \nabla)\mathbf{v}, \boldsymbol{\varphi})_{\Omega^f} - \frac{1}{2}((\mathbf{v}^* \cdot \nabla)\boldsymbol{\varphi}, \mathbf{v})_{\Omega^f} \\
&\quad + \frac{1}{2}((\mathbf{v}^* \cdot \mathbf{n})^+ \mathbf{v}, \boldsymbol{\varphi})_{\Gamma^f_{\mathrm{Out}} \cup \Gamma^f_{\mathrm{In}}}, \\
f(\Phi) &= \frac{1}{2\Delta t}\left(4\overline{\mathbf{v}}^n - \overline{\mathbf{v}}^{n-1}, \boldsymbol{\varphi}\right)_{\Omega^f} + (p_{\mathrm{in}}, \boldsymbol{\varphi})_{\Gamma^f_{\mathrm{In}}},
\end{aligned} \tag{3.6}$$

where $(\alpha)^+$ denotes positive part of real number α, i.e. $(\alpha)^+ = \max\{0, \alpha\}$, and the trilinear form $c(\cdot;\cdot,\cdot)$ represents convection term in skew-symmetric form, see e.g. [13]. This specific form of convection is tied together with the directional do-nothing boundary condition (2.8 b), see [2].

Finite element approximation and its stabilization. The weak formulation (3.5) is discretized by the FEM. In order to prevent numerical instabilities a combination of streamline-upwind/Petrov-Galerkin (SUPG), pressure-stabilization/Petrov-Galerkin (PSPG) and 'div-div' stabilization is used, see [3], [13]. This approach provides robust and accurate numerical method, which is consistent with the original problem. The minielement $\mathrm{P}_1^{\mathrm{bub}}/\mathrm{P}_1$ is used in practical computations, which satisfies the well-known Babuška-Brezzi condition according to [4]. The arising nonlinear system of equations is solved by the Picard iterations.

3.3. Vibroacoustics. The acoustic problem (2.9) is treated similarly. First (2.9) is weakly formulated: Find $p^a \in Y$ such that

$$\left(\frac{1}{c_0^2}\frac{\partial^2 p^a}{\partial t^2}, \eta\right)_{\Omega^a_{\rm prop}} + (\nabla p^a, \nabla \eta)_{\Omega^a_{\rm prop}} = \left(\rho^f \frac{\partial^2 (\mathbf{u}\cdot\mathbf{n}^s)}{\partial t^2}, \eta\right)_{\Gamma_{\rm W_{ref}}}, \tag{3.7}$$

is satisfied for any $\eta \in Y$, where $Y = H^1(\Omega^a_{\rm prop})$.

Further, the space Y is approximated by its FE subspace Y_h and approximate solution p^a_h is sought in the form $p^a_h(X,t) = \sum_{j=1}^{N^a_h} \gamma_j(t)\eta_j(X)$, where η_j are FE basis functions. This leads to the system of ODEs for unknown vector $\boldsymbol{\gamma}(t) = (\gamma_j)$

$$\mathbb{M}^a \ddot{\boldsymbol{\gamma}} + \mathbb{K}^a \boldsymbol{\gamma} = \mathbf{b}^a(t), \tag{3.8}$$

where matrices $\mathbb{M}^a$ and $\mathbb{K}^a$ are the mass and stiffness matrices, respectively, and the components of right hand side vector $\mathbf{b}^a(t) = (b^a_i)$ are given by

$$b^a_i = \left(\rho^f_0 \frac{\partial^2 (\mathbf{u}\cdot\mathbf{n}^s)}{\partial t^2}, \eta_i\right)_{\Gamma_{\rm W_{ref}}}, \tag{3.9}$$

where $\frac{\partial^2 \mathbf{u}}{\partial t^2}(t_n)$ is approximated by the second order central scheme. The acoustic and structure meshes are chosen to be consistent across the interface $\Gamma_{\rm W_{ref}}$.

3.4. Numerical solution of coupled problem. As the influence of acoustic field on the structure deformation is neglected, the FSAI problem decouples into the solution of FSI problem and the acoustic problem with given sound sources at boundary. Thus the numerical solution of FSAI problem consists of following steps:

1) Solve FSI problem. The partitioned approach is implemented in strong version of coupling, so in every time step the inner iteration runs until the convergence of aerodynamic forces is reached, see [13].

2) Prepare sound sources in the form of interface normal acceleration at acoustic mesh nodes lying on the interface $\Gamma_{\rm W_{ref}}$ according to formula (3.9).

3) Solve sound propagation problem given by system (3.8) with prepared sources according to (3.9). The propagation problem is solved on the whole acoustic domain Ω^a, i.e. with included vocal tract model, free field region and PML domain.

4. Numerical experiments.

4.1. FSI results. The vocal fold (VF) model and the fluid domain dimensions, see Figure 4.1 left, is based on the geometric settings published in [15]. The VF model is composed of four layers (with material parameters chosen from [12]) and the initial glottal gap equals to 2.0 mm. Further the point A ($[11.57, -1.50]$ mm) is situated at the top of the bottom VF and used for analysis of numerically simulated VF vibrations.

Analysis of FSI results. The numerical settings were following: the constant time step Δt is chosen as $2.5 \cdot 10^{-5}$ s and $T = 1.0$ s, densities are set to $\rho^s = 1000\,\mathrm{kg/m^3}$ and $\rho^f = 1.185\,\mathrm{kg/m^3}$ and the kinematic fluid viscosity $\nu^f = 1.545 \cdot 10^{-5}\,\mathrm{m^2/s}$. The damping parameters of all VF materials are selected as $\epsilon_1 = 5\,\mathrm{s^{-1}}, \epsilon_2 = 2.0 \cdot 10^{-5}$ s. The VF vibration is excited by the prescribed airflow pressure drop between the inlet $\Gamma^f_{\rm In}$ and the outlet $\Gamma^f_{\rm Out}$ of the value $p_{in} = 1500\,\mathrm{Pa}$. The VFs are released for the interaction after 0.01 s of the computation, when the flow field was already fully developed.

Figure 4.2 illustrates a typical behaviour of the flow induced vibration at the point A. The vibrations with bounded amplitudes show that the chosen $p_{\rm in}$ lies

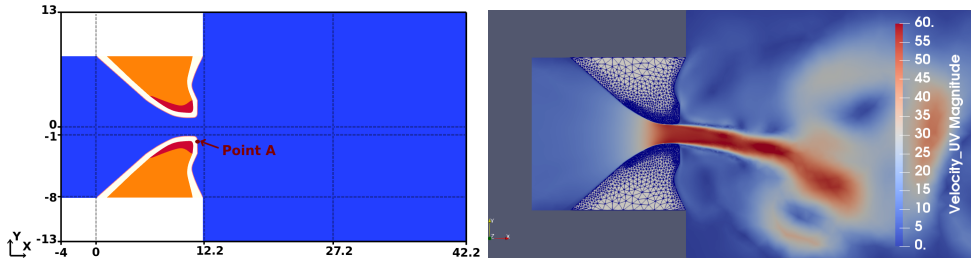

FIG. 4.1. ***Left:*** *The computational fluid and structure domain with dimensions in mm shown. Four different colours mark four layers of vocal fold model, further the location of point A is shown.* ***Right:*** *Magnitude of airflow velocity shown for one time instant.*

below phonation onset pressure threshold, for which unstable VF oscillation (typical for human phonation) appears. The Fourier analysis of the displacement shows two dominant frequencies $f_1 = 121$ and $f_2 = 211\,\mathrm{Hz}$, which agree well with the first two VF eigenfrequencies, see [15]. The typical flow field pattern is plotted in Figure 4.1 right.

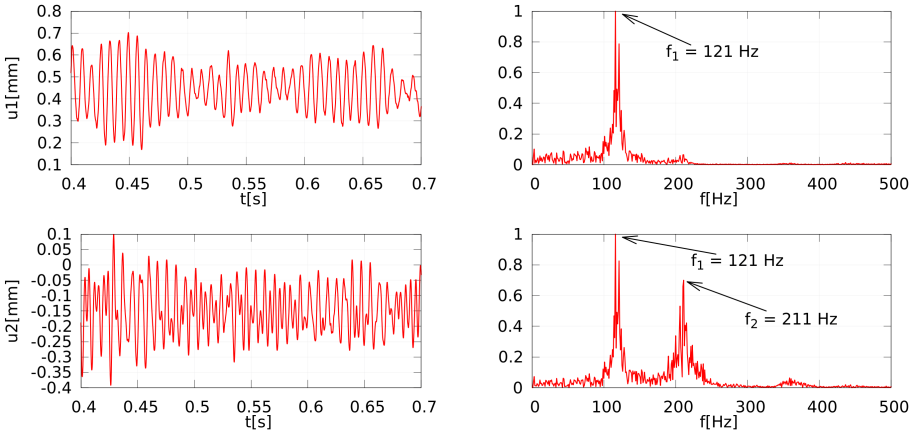

FIG. 4.2. ***Left:*** *The time evolution of displacement of chosen point A in x- and y-direction shown top and bottom, resp.* ***Right:*** *The normalized Fourier transform of the time signal (with full length of* 1 *s) of displacement* u_1 *(top) and* u_2 *(bottom).*

4.2. Vibroacoustics. The vibroacoustics is solved with the known interface vibration determined using the previous FSI numerical solution. The time step is chosen $\Delta t^a = 5 \cdot 10^{-5}\,\mathrm{s}$ and the speed of sound $c_0 = 346\,\mathrm{m/s}$ is considered. A part of acoustic domain Ω^a – the vocal tract model of vowel [u:] is based on the MRI data from [9], with an exception that the total length of vocal tract is longer than in paper [9] due to inclusion of the FSI domain, see [12]. Two microphones B and C are placed at the end of fluid flow domain and 2 cm in front of mouth, respectively, see Figure 2.2.

Vibroacoustic results. The Fourier transforms of acoustic signals measured at both microphones B and C are shown in Figure 4.3. The frequency spectrum of acoustic pressure in point B shows that the dominant frequencies correspond approximately to the first two fundamental frequencies of VF vibration followed by first two resonant

frequencies of vocal tract model (called formants) 283 Hz and 937 Hz. The Fourier transform of signal from point C, i.e. point outside the vocal tract model, exhibits a weakening of frequency 127 Hz (dominant frequency of VF motion) and strengthening of frequencies 937 and 2519 Hz, i.e. the second and the fourth formants.

The sound pressure level (SPL) of sound induced by VF vibration is quite silent reaching circa 20 dB, see Figure 4.4. The first two VF eigenfrequencies (f_1, f_2) are the most dominant frequencies similarly as in [7]. The first two formants (F_1, F_2) are also clearly visible in Figure 4.4, while the third and the fourth formant (F_3, F_4) of vocal tract model is less significant but still present. These formants frequencies do not agree well with the measured formants as reported in [9] due to the prolongation of the acoustic domain.

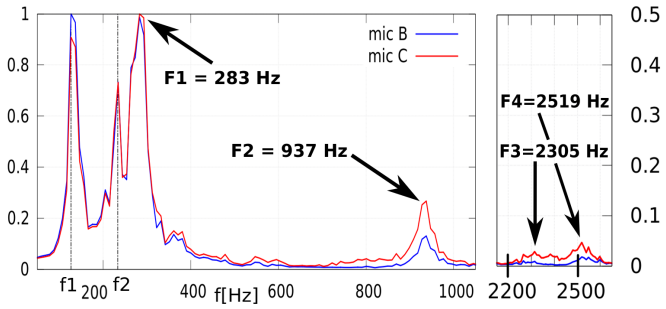

FIG. 4.3. *The normalised Fourier transform of pressure* p^{va} *from the microphones B and C. The frequencies* $f_1 = 127$ *Hz and* $f_2 = 233$ *Hz highlighted by dot lines correspond to the first two dominant frequencies of VF vibration, the other frequency peaks marked by arrows are of acoustic origin. The missed frequency range* $1000 - 2200$ *Hz does not contain any resonant frequencies. The right part of the figure has different scaling.*

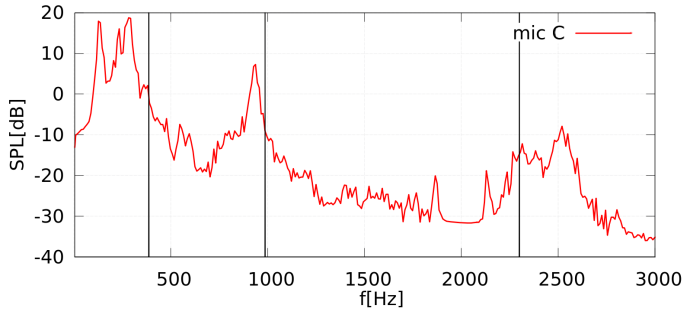

FIG. 4.4. *The sound pressure level in frequency domain computed at the point C. The black vertical lines demonstrate first three formants with frequencies* 389 Hz, 987 Hz *and* 2299 Hz *taken from article [9]. The acoustic signal outside mouth shows quite low SPL of sound with vibration origin against SPL of sound with aerodynamical origin, see e.g. [6]. This can be different with use of a model with VF contact, see [10].*

5. Conclusion. The mathematical model of the FSAI problem representing vibroacoustic problem of human phonation was described and it was numerically approximated by the (stabilized) FEM. The acoustic problem was decoupled from the FSI part. The acoustic pressure simulation of the vowel [u:] phonation was performed

and the frequency spectra show that the first two VF eigenfrequencies as well as the first two formants are dominant. The resulting SPL in front of mouth based on the FSI simulation without VF contact is quite low compared to the results in [7].

Acknowledgments. The financial support of this study was provided by the Czech Science Foundation under the Grant No. GA 19-04477S and by the Grant No. SGS19/154/OHK2/3T/12 of the Grant Agency of the CTU in Prague.

REFERENCES

[1] F. Alipour, C. Brucker, D. D Cook, A. Gommel, M. Kaltenbacher, W. Mattheus, L. Mongeau, E. Nauman, R. Schwarze, I. Tokuda, et al., *Mathematical models and numerical schemes for the simulation of human phonation*, Current Bioinformatics **6**:3 (2011), 323–343.

[2] M. Braack and P. B. Mucha, *Directional do-nothing condition for the Navier-Stokes equations*, Journal of Computational Mathematics **32** (2014), 507–521.

[3] M. Feistauer, P. Sváček, and J. Horáček, *Numerical simulation of fluid-structure interaction problems with applications to flow in vocal folds*, Fluid-structure Interaction and Biomedical Applications (T. Bodnár, G. P. Galdi, and S. Nečasová, eds.), Birkhauser, 2014, pp. 312–393.

[4] V. Girault and P. A. Raviart, *Finite element methods for Navier-Stokes equations*, Springer-Verlag, 1986.

[5] B. Kaltenbacher, M. Kaltenbacher, and I. Sim, *A modified and stable version of a perfectly matched layer technique for the 3-D second order wave equation in time domain with an application to aeroacoustics*, Journal of Computational Physics **235** (2013), 407–422.

[6] M. Kaltenbacher, *Numerical simulation of mechatronic sensors and actuators: finite elements for computational multiphysics*, Springer, 2015.

[7] M. A. Lodermeyer, *A laser-based technique to evaluate sound generation during phonation*, Ph.D. thesis, Friedrich-Alexander-Universität Erlangen-Nürnberg, 2019.

[8] W. S. Slaughter, *Linearized elasticity problems*, Springer, 2002.

[9] B. H. Story, I. R. Titze, and E. A. Hoffman, *Vocal tract area functions from magnetic resonance imaging*, The Journal of the Acoustical Society of America **100**:1 (1996), 537–554.

[10] P. Sváček and J. Valášek, *Mathematical modelling and numerical simulation of flow induced vibrations of vocal folds model with collisions*, AIP Conference Proceedings, vol. 2116, AIP Publishing, 2019, p. 030003.

[11] I. R. Titze, *Principles of voice production*, Prentice Hall, 1994.

[12] J. Valášek, M. Kaltenbacher, and P. Sváček, *On the application of acoustic analogies in the numerical simulation of human phonation process*, Flow, Turbulence and Combustion (2018), 1–15.

[13] J. Valášek, P. Sváček, and J. Horáček, *On suitable inlet boundary conditions for fluid-structure interaction problems in a channel*, Applications of Mathematics **64**:2 (2019), 225–251.

[14] W. Zhao, C. Zhang, S. H. Frankel, and L. Mongeau, *Computational aeroacoustics of phonation, part I: Computational methods and sound generation mechanisms*, The Journal of the Acoustical Society of America **112**:5 (2002), 2134–2146.

[15] S. Zörner, M. Kaltenbacher, and M. Döllinger, *Investigation of prescribed movement in fluid-structure interaction simulation for the human phonation process*, Computers & Fluids **86** (2013), 133–140.